Morphological evolution and surface and interface structure of aluminum on polyimide

Xue-Feng Lin[a)]
Charles Evans & Associates, 810 Kifer Road, Sunnyvale, California 94086

David A. Grove
Luxel Corporation, 515 Tucker Avenue, Friday Harbor, Washington 98250

Lun-Cun Wei and Greg S. Strossman
Charles Evans & Associates, 810 Kifer Road, Sunnyvale, California 94086

Glenn Lefever-Button
Luxel Corporation, 515 Tucker Avenue, Friday Harbor, Washington 98250

Jeffrey R. Kingsley
Charles Evans & Associates, 810 Kifer Road, Sunnyvale, California 94086

(Received 7 September 2001; accepted 11 February 2002)

Al growth and nucleation on polyimide and the resultant surface morphologies and interfacial structures have been investigated by atomic force microscopy, focused ion beam scanning electron microscopy, Rutherford backscattering spectroscopy, and x-ray photoelectron spectroscopy. Al growth on polyimide proceeds in a two-dimensional-like mode. Initial Al deposition results in the formation of nanoparticles, exhibiting the interface structures arising from the Al interacting with the carbonyl groups of the polyimide. Subsequent Al growth produces a landscape of crystallized islands, and these islands have submicrometer dimensions with different orientations. © *2002 American Vacuum Society.* [DOI: 10.1116/1.1467658]

I. INTRODUCTION

Polyimides have attracted increasing attention mainly due to their microelectronic applications. The characteristic properties of polyimides include high thermal stability, reliable mechanical strength, and low dielectric constants. These properties are critically important when packaging metal–insulator multilayered structures of metals and polymers on semiconductor chips. Since interfacial structures usually play a key role in influencing these properties, better manipulation and characterization of these properties have motivated many studies aimed at understanding metal–polymer interfaces.[1,2]

In the past few years, a variety of techniques have been employed to study the chemistry of metal–polymer surfaces and interfaces and the mechanisms of interfacial structure formation. Metal/polyimide interfacial structures have been observed on several different metal/polyimide compounds. Specifically, Al, Cr, Ni, and Ti atoms strongly interact with the carbonyl groups (C═O) of the polyimides, giving rise to the interfacial structures for initial stages of metal growth. Cu/polyimide systems are an exception in which no strong interaction between Cu and carbonyl groups of the polyimides has been observed, and Cu atoms usually migrate or diffuse into polyimides forming metal clusters.[1–10]

Compared with extensive studies on the deposition kinetics and interfacial electronic structures, surface morphology and surface structures of thin films formed from metals deposited onto polyimides have been less well systematically characterized, and relatively little attention has been devoted to these investigations. We have noticed that there have been several previous publications mentioning surface morphology studies. For example, *Wickland* and co-workers have studied thermal chemical vapor deposited Al on polyimides coated with the TiN thin films, and focused on exploring chemical composition, surface morphology, and adhesion characteristics of the formed films.[11] Other studies have concentrated on examining the effects of either thermal cycling or ion irradiation on metal/polyimide surface topographies.[12–14] *Silvain* and colleagues used transmission electron microscopy (TEM) to characterize surface morphologies of metals grown on polyimides, but their study emphasized identifying different growth behavior of Al and Cu.[15]

Surface structures and morphologies of metal growing on polyimides not only affect surface electronic structures but also significantly influence the chemical, mechanical, and electronic properties. In this article, we report our results of Al thin films growing on polyimide by using several different characterization techniques. The objective of this research is to study Al growth, nucleation, and surface and interfacial structures on polyimide. Atomic force microscopy (AFM) and Rutherford backscattering spectroscopy (RBS) were used to monitor surface morphological evolution and variations of depth profiles and stoichiometries of the Al/polyimide film complex as a function of Al film thickness. Compared with previous TEM measurements of the Al/polyimide film complex, AFM studies of surface morphology can give both high surface sensitivity and high resolution of surface structures. Also, since the surfaces of the polyimide before and after growing the Al thin films are

a)Electronic mail: xlin@cea.com

 ©2002 American Vacuum Society

nonconducting or rough on the nanometer-scale, AFM is the preferred technique for investigating the morphological variations of polyimide at different stages of Al growth. X-ray photoelectron spectroscopy (XPS) and focused ion beam scanning electron microscopy (FIB-SEM) were also used to obtain chemical bonding and geometric structures at the interface formed between Al and polyimide.

Examining the variations of surface topographies at both early and later stages of Al depositing on polyimide and investigating the interfacial structures will provide a more complete picture for the development of the prominent surface characteristics associated with Al growing on polyimide, such as chemisorption, nucleation, growth, etc. This will help improve the understanding of physical and chemical properties of the metallized polymers.

II. EXPERIMENTAL PROCEDURES

A. Sample preparation

The polyimide used for this study is Hitachi PIQ-L100 biphthalic dianhydride (BPDA/PPD) diluted 50% by weight solution in *N*-methylpyrrolidinone. Film preparation follows standard spin casting methods on Si (100) oriented wafers. No surface modification was used on these wafers prior to spinning. Following casting, the films were thermally imidized with an initial "soft bake" at a nominal temperature of 100 °C to remove solvents. Following soft bake, the polyiamic acid was thermally imidized in a partial vacuum dry nitrogen environment with a maximum temperature of 325 °C. Polyimide film thickness was determined using a Dektak 3ST surface profilometer.

At a vacuum pressure of 3×10^{-6} Torr, the aluminum was e-beam evaporated onto the substrate coated with polyimide films. Deposition rate and thickness were monitored and controlled by a Leybold-Inficon IC5 deposition controller, with a nominal incident rate at the substrate of 10 Å/s. To ensure film thickness uniformity, the substrates with polyimide films were rotated in a planetary motion above the Al source. The deposited Al thickness was also calibrated using a Dektak 3ST surface profilometer.

B. AFM

Surface morphologies were examined using a Digital Instruments Nanoscope III multimode AFM. The AFM was operated in a tapping mode, and images were acquired at both height and phase mode. A commercial silicon cantilever (length 100 um, spring constant 42.0 N/m) with an integrated pyramidal tip (size less than 10 nm) was used, combined with a laser level detection technique. All AFM measurements were performed on the surfaces in air at room temperature. Surface particles and islands were analyzed for each image, and the surface roughness was measured in the height images. The average height of the islands or features on the surface was also calculated. All AFM images shown here were processed by leveling and contrast adjustment.

C. RBS

Under a vacuum pressure of low 10^{-6} Torr, RBS spectra were acquired at backscattering angles of 160° and 110° with the sample perpendicular to the incident 2.275 MeV He^{++} ion beam. The experimental parameters have been chosen to optimize the signal from the deposited Al layer. The different depth resolution and backscattering kinematics afforded by the use of different detection angles improve the accuracy of the analysis for both thickness and stoichiometry. In addition, channeling of the substrate Si allows a more precise determination of the N, O, and C concentrations.

D. FIB-SEM

Cross sectioning and imaging of the sample was performed in an FEI DualBeam Model 830 FIB at a vacuum pressure of $\sim10^{-8}$ Torr, using a primary ion beam voltage of 30 kV. Once sectioned, the field emission scanning electron microscope (FE-SEM) was used to image the sample. No tilt correction was made during the acquisition of the images. By tilting the sample forward we should be able to work with the top surface without charging. It will be best to work at the highest voltage possible to get as much of the beam through the sample.

E. XPS

XPS data were collected on a Physical Electronics Quantum 2000 using a Monochromated Al K_α 1486.6 eV x-ray source. The take-off angle was 45°. The acceptance angle was ±23°.

Depth profiling was accomplished by alternating sputter etching and data acquisition cycles. In order to minimize crater roughening and smearing of the interfaces, Zalar rotation was employed during the sputter etching. A 4 keV Ar^+ beam rastered over a 4 mm×4 mm area was utilized to sputter quickly through most of the Al layer. Just before the interface, sputter conditions were changed to 1 keV Ar^+, 4 mm×4 mm, in order to minimize damage in the interface region.

Quantification (atomic concentration) of electron spectroscopy for chemical analysis (ESCA) data relies on relative sensitivity factors and assumes a homogeneous distribution of elements within the analysis volume. The analysis volume is the product of the analysis area (spot size or aperture size) and the depth of information. Photoelectrons are generated within the x-ray penetration depth (typically many microns), but only the photoelectrons within the top three photoelectron escape depths are detected. Escape depths are on the order of 15–35 Å, which results in an analysis depth of ~50–100 Å.

III. RESULTS

A. AFM analysis

Figure 1 shows five characteristic AFM height images of the surfaces of polyimide with nominally 0 Å (a), 10 Å (b), 20 Å (c), 1100 Å (d), and 1300 Å (e) Al thin films coating,

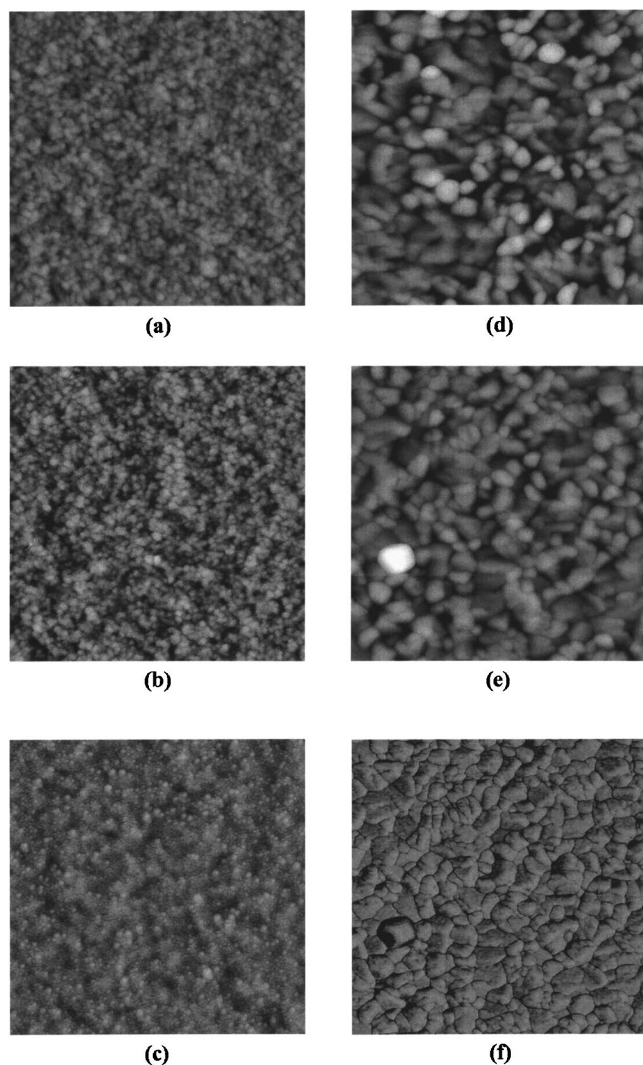

FIG. 1. Five characteristic AFM height images (1×1 μm) of the surfaces with nominally 0 Å Al / 630 Å polyimide (a), 10 Å Al/660 Å polyimide (b), 20 Å Al/670 Å polyimide (c), 1100 Å Al/800 Å polyimide (d), and 1300 Å Al/400 Å polyimide (e) thin films growth, respectively, showing the surface morphology evolution with increasing Al film thickness. A phase image (1×1 μm) in (f) was simultaneously taken with the height image [(e)] on the same surface location, showing the oriented islands.

respectively. The image in Fig. 1(a) shows surface topography before Al deposition, serving as a reference to monitor the variations of the surface structures arising from the Al growth. The last four images in Figs. 1(b)–1(e) demonstrate the surface morphologies at the early and later stages of Al deposition. The brighter and darker contrasts in the images represent the higher and lower surface features, respectively.

The clean surface of the polyimide without Al deposition shows a rough landscape of clusters [Fig. 1(a)]. These clusters are roughly round in shape with different sizes. A cross-section measurement indicates that these clusters laterally range from 175 to 550 Å, with the vertical extensions between 4 and 28 Å. On some brighter surface areas, several clusters either appear closer to each other or residing on the underlying clusters, showing a strong contrast compared to the dark surface areas with the scattered clusters. These are

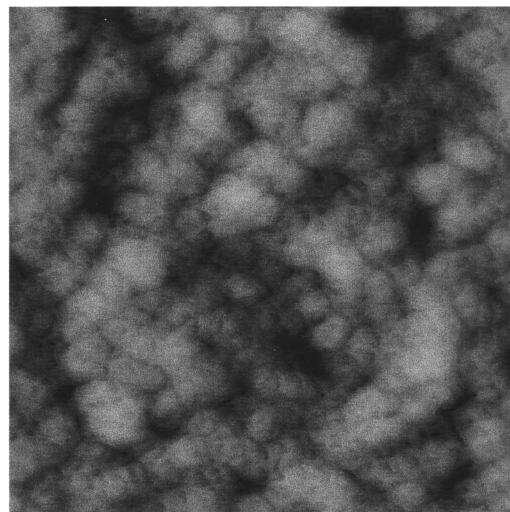

FIG. 2. High resolution AFM height image (0.25×0.25 μm) of the surface with 10 Å Al grown on 660 Å polyimide, showing nanoparticles condensing into clusters.

characteristics of this rough surface. The mean roughness of the surface is 5.66 Å. The rough landscape of the clusters might be correlated to the specific chemistry of polyimides and Si substrates used for polyimide growth. Of course, the sample preparation condition is another important factor that influences the formation of surface structures. We note that several AFM studies have been previously carried out to examine both surface topographies of different polyimides and the effects of surface chemistry and substrate, as well as the sample preparation condition, on the surface morphologies of polyimides.[16–21]

In comparing surface structures of clean polyimide in Fig. 1(a) with that of 10 Å Al deposited on the polyimide in Fig. 1(b), we see overall similar surface cluster landscapes and sizes. However, a closer inspection reveals a difference in the images of these features. In Fig. 1(b), each cluster is composed of small particles. These small particles are clearly seen in a smaller-scale image in Fig. 2, which was taken in a zooming mode on the same surface shown in Fig. 1(b). The small particles exhibit a relatively uniform lateral dimension of about 70 Å, with a vertical extension on the order of about 45 Å. These nanoparticles appear disordered within each cluster. We estimate that each cluster is composed of about 7 particles. Nanoparticles condense into larger clusters with relatively regular sizes; this is associated with the growth of Al thin films. It is observed that there is a tendency for the clusters to grow and coalesce with each other. The mean roughness of this surface is 6.05 Å.

As the Al film thickness is increased [Fig. 1(c)], a similar landscape to the rough surface shown in Figs. 1(a) and 1(b) is visible. However, each individual cluster becomes blurred. It appears that the nanoparticles enlarge and cover the whole surface when compared with those observed in Figs. 1(a) and 1(b), where there are some dark surface areas without the small clusters. These indicate an initial coalescence of the clusters in the film. The particles have larger lateral dimen-

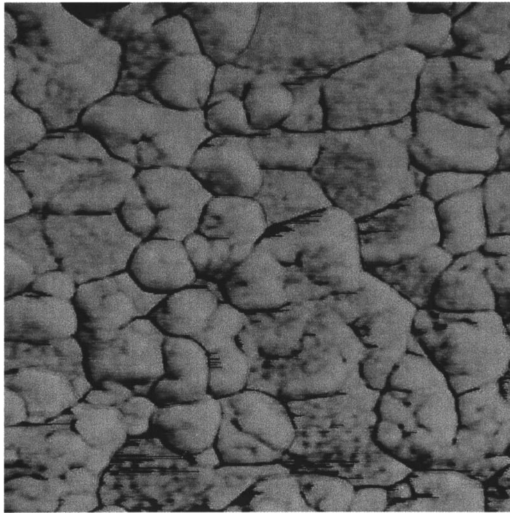

FIG. 3. AFM phase image (0.5×0.5 μm) of the surface with 1300 Å Al grown on 400 Å polyimide, showing small particles residing within the islands.

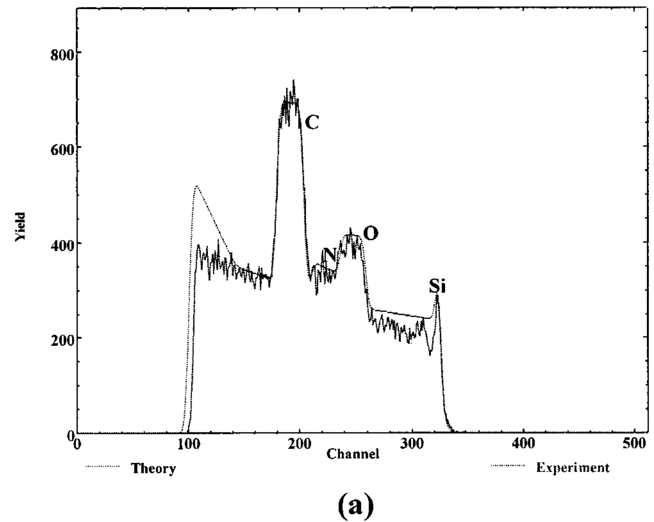

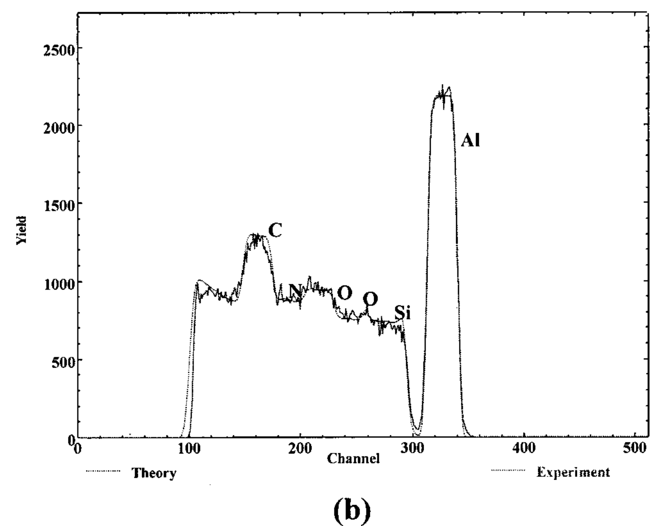

FIG. 4. Two typical RBS spectra taken on the Si samples coated with 630 Å polyimide (a), and 1100 Å Al grown on 800 Å polyimide (b), respectively, showing variations of C, O, N, and Al spectra before and after the Al growth.

sions in the range from 95 to 320 Å and higher extensions between 5 and 250 Å. It is also observed that some individual bright large features are present on the surface, and these features are surrounded by small particles, indicating that the clusters nucleate and grow. The mean roughness of this surface is 5.73 Å.

Increasing the Al film thickness still further to 1100 Å [Fig. 1(d)] and 1300 Å [Fig. 1(e)] produces a landscape of individual islands or grains on the surfaces. Overall, together with irregular sizes, these islands often appear disorganized. These could be easily identified from the depressions or boundaries that distinguish the different islands or grains. These islands exhibit lateral dimensions ranging from 330 to 1330 Å, with vertical extensions between 200 and 344 Å. Some of the islands have a regular shape and flat top, representative of the crystalline structures. Two typical crystalline orientations within these islands could be observed from strong contrast changes and grain boundary distributions, where the two oriented surface planes on different islands appear tilted in two directions. The oriented islands could be easily identified in a phase image shown in Fig. 1(f), which was simultaneously taken with the height image [Fig. 1(e)] at the same surface location. A bright island seen on the lower left side of the image shows a square shape and flat top, and five different faceted planes could be observed. The lateral and vertical dimensions of this island are 1330 and 344 Å. The mean roughness of these two surfaces is 15.27 [Fig. 1(d)] and 33.84 Å [Fig. 1(e)], indicating that the island structures become more prominent with increasing Al growth.

The surfaces of the islands are composed of small particles. Figure 3 shows the fine structures of these particles within the islands. This phase image was taken in a zooming mode on the same surface as shown in Figs. 1(e) and 1(f), and the particles within each island on the surface is clearly visible. The particles appear to have a regular round shape, with about 140 Å lateral dimension and about 10 Å vertical extension. The particles are disordered, and an average interdistance of center to center is measured to be 160 Å. We think that these small particles are most likely the nucleated Al oxide, as will be discussed later. The islands show a variety of lateral dimensions and vertical extensions and the particles within each island display no periodicity. It is impossible to identify specific orientations of the facet planes within the crystalline islands [Figs. 1(d) and 1(e)].

TABLE I. 630 Å polyimide on Si.

Depth (Å)	Atomic concentration				Density (at/cc)
	C	N	O	Si	
<630	76.0	8.8	15.2	···	1.09×10^{23}
630–650	···	···	···	100	5.00×10^{22}
>650	···	···	···	100	5.00×10^{22}

TABLE II. 10 Å Al on /660 Å polyimide on Si.

Depth (Å)	Atomic concentration					Density (at/cc)
	C	N	O	Al	Si	
<10	⋯	⋯	⋯	100	⋯	6.02×10^{22}
10–670	76.9	8.5	14.6	⋯	⋯	1.09×10^{23}
670–700	⋯	⋯	⋯	⋯	100	5.00×10^{22}
>700	⋯	⋯	⋯	⋯	100	5.00×10^{22}

TABLE IV. 1100 Å Al/800 Å polyimide on Si.

Depth (Å)	Atomic concentration					Density (at/cc)
	C	N	O	Al	Si	
<30	⋯	⋯	60.0	40.0	⋯	6.68×10^{22}
30–1130	⋯	⋯	⋯	100	⋯	6.02×10^{22}
1130–1930	76.8	8.1	15.1	⋯	⋯	1.09×10^{23}
1930–1970	⋯	⋯	⋯	⋯	100	5.00×10^{22}
>1970	⋯	⋯	⋯	⋯	100	5.00×10^{22}

B. RBS analysis

To quantify the depth and composition of Al/polyimide films shown in Figs. 1(a)–1(e), RBS spectra were acquired on each sample. The experimental data was fit to a theoretical model by manipulating several parameters in this model. This model simultaneously fits the normal and grazing detector spectra to represent the physical and chemical structures of Al/polyimide. The adjusted parameters include, among others, atomic concentrations and different stoichiometries. Figures 4(a) and 4(b) show two typical RBS spectra taken on the Si samples coated with 630 Å polyimide [Fig. 1(a)], and 1100 Å Al on 800 Å polyimide [Fig. 1(d)], and these spectra exhibit variations of depth profile and stoichiometries of the films due to Al growth. In Fig. 4, the solid lines and dotted lines represent experimental and theoretical results, respectively.

Spectra in Fig. 4(a) taken on pure polyimide spin-coated onto an Si substrate show four distinct features, representing C, N, O, and Si. The first three ones are characteristic of the polyimide films and the fourth corresponds to the Si substrate. A ratio of the C, N, and O is determined to be 76%, 8.8%, and 15.2%, as listed in Table I. These data are consistent well with 78.6%, 7.1%, and 14.3% calculated from the chemical formula of BPDA/PPD polyimides. By including H, the ratios of C, N, O, and H are estimated to be 61.1%, 5.6%, 11.1%, and 22.2%, respectively.

In spectra taken on Al deposited on polyimide [Fig. 4(b)], we see two additional features, labeled Al and O. The pure Al layer is detected on the top of the C, O, and N in the polyimide. The surface O is acquired on the Al layer, implying Al oxidation at the outer part of the layer. The results are indicated in Table IV.

Depth profiles and chemical compositions of all samples shown in Figs. 1(a)–1(e) are summarized in Tables I–V. For comparison, we also show the RBS results of 900 Å Al grown directly on the oxide Si substrate in Table VI, where no C and N were detected. The results in Tables II–V indicate that the deposited Al resides on the polyimide films and the Al does not diffuse into the polyimide to form metal clusters. This is consistent with previous studies.[1–10,15] At high metal film thickness Tables IV–VI show the oxidation of Al surfaces, and the oxide thickness is about 30, 40, and 20 Å, respectively. The thickness of Al oxide layers increases with increasing Al deposition. The formation of oxide layers is due to the fact that after coating Al in the vacuum, the sample had been taken out and exposed in air. However, this surface Al oxide is not clearly seen at the initial stages of 10 Å and 20 Å Al deposited on the polyimide, as shown in Tables II and III. We think that two factors play key roles here. First, the deposited Al at the initial stages interacts with carbonyl groups of the polyimide and forms an interface, and the surface appears terminated by the interfacial structures associated with Al–O–C complex, as will be discussed later. Second, the deposited Al layer at the initial stages is so thin that the RBS detection could not distinguish the oxygen in the polyimide from that in the Al oxide.

Tables I–V show that there are slight variations of the C, O, and N concentrations in the polyimide. We think that these changes probably arise from the RBS detection uncertainty. The measured data errors fall in the range of the RBS detection limits, and it is hard to correlate these small changes to the Al deposition with different film thickness.

C. FIB-SEM analysis

FIB-SEM was used to reveal the structures of Al/polyimide interface. Figure 5 presents the cross-sectional FE-SEM image of 1600 Å Al deposited on 1100 Å polyimide on a Si substrate. The sample was tilted to 52° in order to observe the structures of both the surface and cross section of the films. Surface topography appears similar to those seen on the surfaces presented in Figs. 1(d) and 1(e). The cross-section structures of the Al layers/polyimide films on the Si substrate could be resolved from contrast changes in the im-

TABLE III. 20 Å Al/670 Å polyimide on Si.

Depth (Å)	Atomic concentration					Density (at/cc)
	C	N	O	Al	Si	
<20	⋯	⋯	⋯	100	⋯	6.02×10^{22}
20–690	76.0	8.8	15.2	⋯	⋯	1.09×10^{23}
690–710	⋯	⋯	⋯	⋯	100	5.00×10^{22}
>710	⋯	⋯	⋯	⋯	100	5.00×10^{22}

TABLE V. 1300 Å Al/400 Å polyimide on Si.

Depth (Å)	Atomic concentration					Density (at/cc)
	C	N	O	Al	Si	
<40	⋯	⋯	60.0	40.0	⋯	6.68×10^{22}
40–1340	⋯	⋯	⋯	100	⋯	6.02×10^{22}
1340–1740	78.0	8.1	13.9	⋯	⋯	1.09×10^{23}
>1740	⋯	⋯	⋯	⋯	100	5.00×10^{22}

TABLE VI. 900 Å Al on Si oxide.

Depth (Å)	Atomic concentration O	Al	Si	Density (at/cc)
<20	60.0	40.0	⋯	6.68×10^{22}
20–920	⋯	100	⋯	6.02×10^{22}
920–940	60.0	40.0	⋯	6.68×10^{22}
>940	⋯	⋯	100	5.00×10^{22}

age. The lower part of the image exhibits the cross section of the Si substrate, and polyimide films reside between the Si substrate and Al layers. Slight variations in the thickness of the Al layer and a typical columnar grain structure of the cross-section Al layer is observed, but detailed structures of cross-sectioned polyimide films are unclear. A well-defined interface between the Al layer and polyimide is resolved and tiny changes in the thickness of the interface layer are visible. The average thickness of the interface layer is measured to be 113 Å. A close examination reveals slight contrast variations at the outmost layers of Al films, and these probably arise from the formation of Al oxide. However, it is difficult to determine the thickness of this Al oxide layer in this image.

D. XPS analysis

Surface analysis and a depth profile, both using XPS, were undertaken to investigate chemical bonding at the surface and at the Al/polyimide interface, respectively. The depth profile and surface analysis were taken on the previously discussed sample with 1100 Å Al deposited on 800 Å polyimide on Si. Figure 6 shows elemental data from the depth profile. Photoelectron spectra from carbon, nitrogen, oxygen, and aluminum are shown in montage format, with the elemental peak intensities and binding energies plotted as a function of sputter cycle. In the plots, point "0" represents the unsputtered surface and the profile propagates along the z axis, and the z directions in Figs. 6(a) and 6(b) are plotted to be opposite to these in Figs. 6(c) and 6(d) in order to clearly see the evolution of the spectra. For convenience, in Fig. 6 we identify the surface, Al layer, interface, and polyimide regions by "I–IV," respectively.

On the surface (defined by an XPS sampling depth of ~ 50 Å) indicated by "I," the centroid of the broad O $1s$ peak is seen at ~ 531.5 eV [Fig. 6(c)]. The O peak includes contributions from surface organic species (adventitious hydrocarbons) as well as oxidized Al. Two distinct peaks in the Al $2p$ spectrum [Fig. 6(d)] are indicative of Al metal (71.37 eV) and Al oxide (74.51 eV), confirming the presence of a native oxide growth on the surface of the Al [Fig. 7(a)]. This native surface oxide is consistent with the RBS results.

Carbon levels on the surface of the Al film are likely to be entirely due to adventitious carbon from atmospheric exposure [Fig. 6(a)], and the N $1s$ line is barely detected on the surface [Fig. 6(b)]. C, O and N were not detected within the bulk of the Al film as labeled by "II." Similarly, the Al spectrum from within the Al film shows a single asymmetric peak that is consistent with Al metal.

Some interesting features are observed in the interface region between the Al and polyimide, as labeled by "III." The interface region is clearly seen in each of the spectral windows, either by increasing (C, O, and N) or decreasing (Al) peak intensities. Within the interface region, the Al peak shows additional structure that indicates the presence of mul-

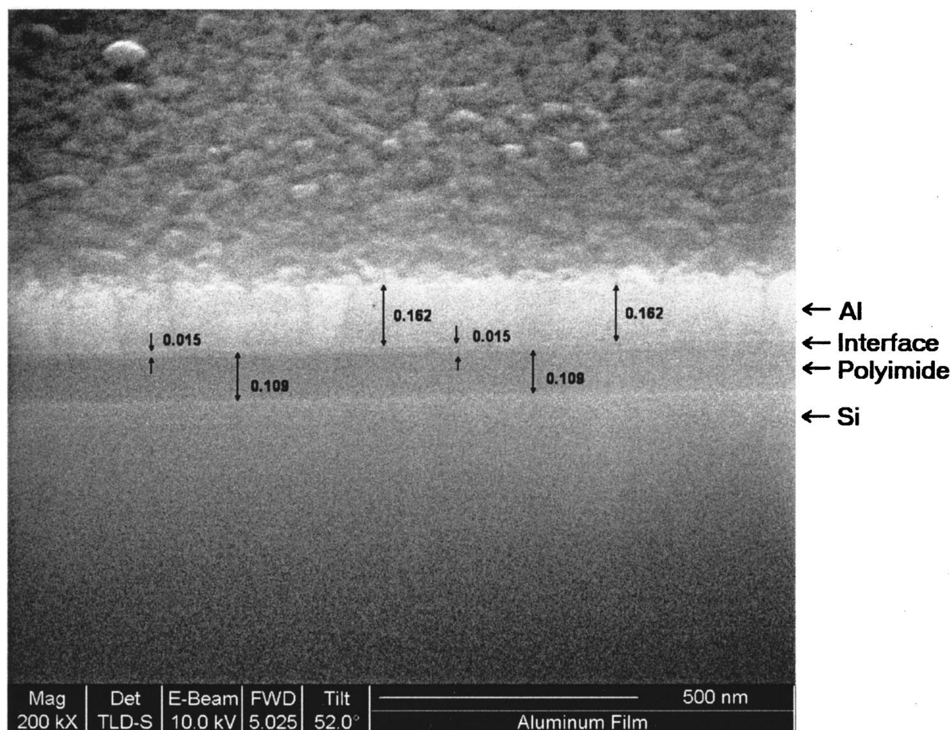

FIG. 5. FIB-SEM image of cross-section structures of the Si sample with 1600 Å Al deposited on 1100 Å polyimide, showing the interface between the Al layer and the polyimide films. The Al layer, the interface, the polyimide film, and the substrate Si are indicated.

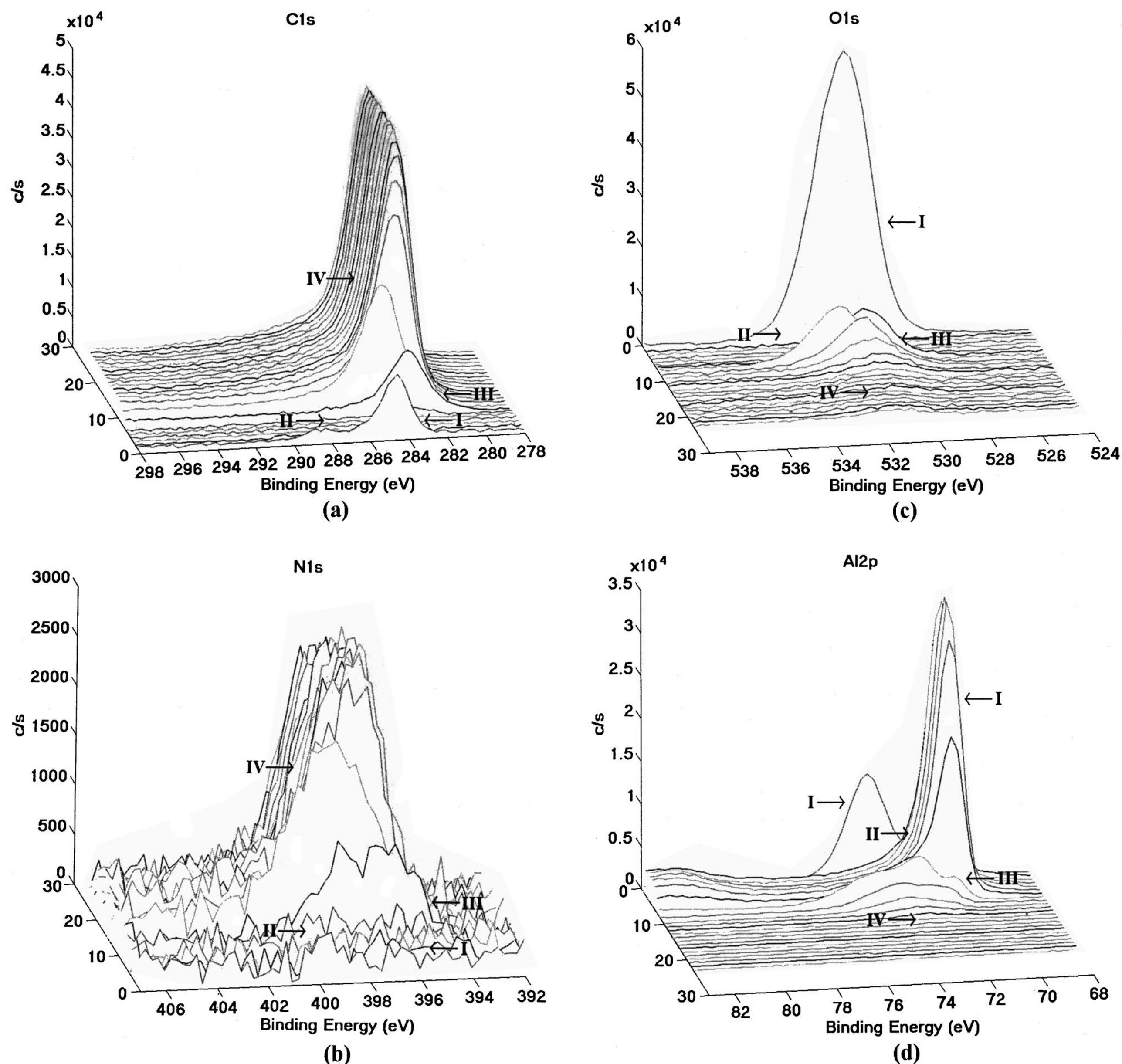

FIG. 6. Evolution of the core-level spectra of C 1*s*, N 1*s*, O 1*s*, and Al 2*p* starting from the surface down to the inside polyimide as a function of sputtering cycle. The sample was 1100 Å Al grown on 800 Å polyimide film. The spectra taken on the surface, the Al layer, the interface, and the polyimide are indicated by I–IV, respectively.

tiple bonding states. Figure 7(b) shows the results of a nonlinear least squares curve fit of the Al peak within the interface region. Along with the Al metal peak (seen here at ~71.37 eV binding energy), three additional curves were fit under the peak. The most intense band, observed at a 1.48 eV shift above the Al metallic state, is consistent with Al interacting with carbonyl groups in the polyimide; as has been previously assigned in the literature.[1–10] Corresponding binding energy shifts in the C 1*s*, N 1*s*, and O 1*s* peaks at this point in the profiles are further indication of the interaction between Al and the polyimide (Fig. 6). Specifically, the deposited Al adatoms break the C=O double bonds and form an Al–C–O complex, and this reaction is accompanied by a charge transfer from Al to C.[1–10]

The two remaining Al peaks with higher binding energy shifts in Fig. 7(b) are likely associated with Al oxide and/or hydroxide states. The exact binding energies of these bands, or their shifts from the binding energy of the metallic state may not reflect familiar literature values due to the transition from a conductive metal film to a semi-insulating interface transitioning further into a bulk insulator (insulating polyimide).

Inside the polyimide as labeled by "IV," we see that the C 1*s* and N 1*s* line appear asymmetric and sharp, with the major peaks located at 284.85 and 398.79 eV. The decreasing O 1*s* peak intensity trends with the Al 2*p* peak within the interface until reaching a steady-state intensity within the polyimide. The Al 2*p* line shows no indication of detectable

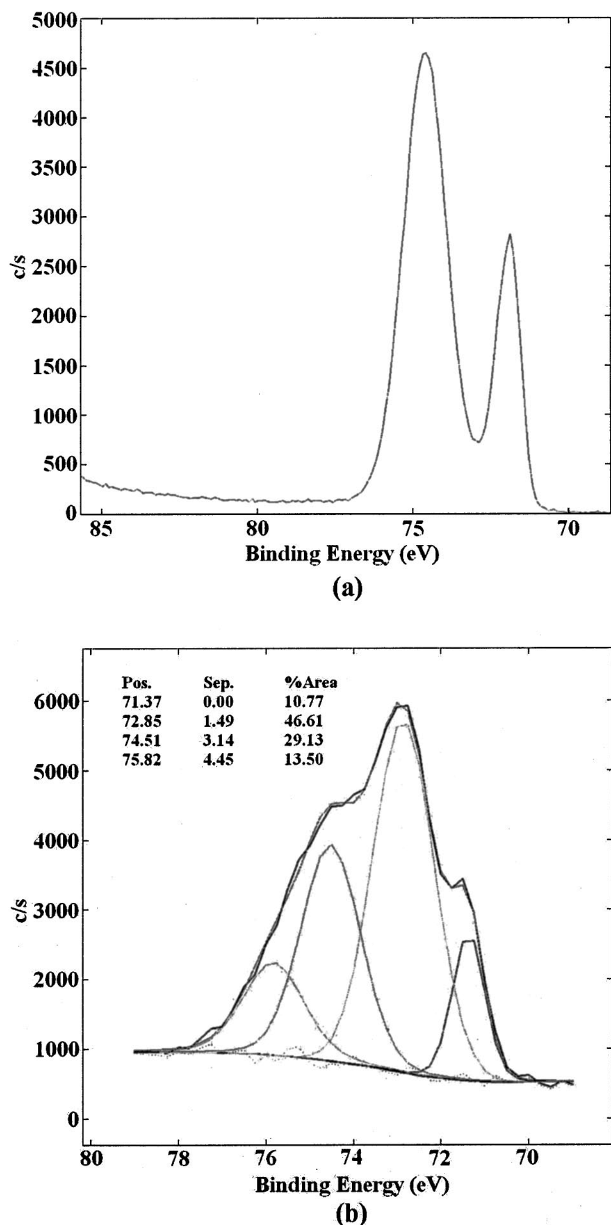

FIG. 7. (a) Al $2p$ line acquired on the surface, indicative of the Al metal and Al oxide. (b) A nonlinear least squares curve fit of the Al peak within the interface region, showing four features. The key feature at 72.85 eV arising from the Al–C–O complex.

levels of Al within the polyimide, indicating that there is no metal clustering in the polyimide. These results are consistent with the RBS measurements from this sample.

IV. DISCUSSION

The images in Figs. 1(b)–1(e) outline surface structures at the early and later stages of Al growth. The surface topography of polyimide before Al growth shows a landscape of clusters, which might be of crystalline-like structures or some polyimide aggregations. At the early stages of Al growth, the topographic structures of these films in AFM images contain features on at least two scales. The large-scale topography gives the overall impression of roughness and shows inhomogeneities such as clusters and boundaries. Higher resolution analysis often resolves fine structures consisting of nanoparticles within the clusters.

Several nanoparticles condense into clusters, and atomic corrugation is not resolved within these nanoparticles. This is indicative of a two-dimensional (2D) close-packed structure [Figs. 1(b) and 2]. We think that these nanoparticles are probably nucleated Al carbon-oxide rather than the agglomerated Al adatoms. The reason for this is quite simple. First, as indicated in the XPS study, the deposited Al interacts with carbonyl groups of the polyimide to break C=O double bonds and form Al–C–O complex. Second, AFM measurements were performed in air and Al adatoms on the polyimide would be oxidized even if they did not show the Al–O–C complex.

The landscape of the nanoparticles is ascribed to the limited mobility or diffusion of the deposited Al adatoms due to interaction between the adsorbate and substrate, i.e., Al–O–C complex interactions, as we see in the XPS study. These complexes grow nuclei initially with relatively high probability of the nuclei fusing into clusters separated by grooves and depressions before a film coalesces [Fig. 1(b)]. Subsequent coating of the Al adatoms on the surface leads to a coalescence of these particles or clusters [Fig.1(c)], indicating a phase transition from agglomerated small particles into clusters. The surface irregularities of Al–O–C complex films are likely correlated to the morphology of the polyimide substrate, and the formed thin film reflects the shape of the surface topography from which it grows.

As the film thickens, the Al adatoms within the clusters will feel an increasing surface stress arising from the adsorbate–adsorbate interactions. In order to be energetically favorable, it is possible that above a critical dimension the clusters will stop growing together and form the islands of crystalline structures. As can be seen in Figs. 1(d) and 1(e), the topographies of the surfaces are little changed on a large scale. The Al crystalline islands are also visible from the columnar structures seen in Fig. 5.

To confirm the growth behavior of Al on polyimide, at each deposition stage we took AFM images on a much larger scale at different surface locations. Overall, the surfaces appear relatively flat at these larger scales and we did not observe the prominently larger features or islands which are distinguished in size and shape from those seen on the surfaces at each of the growth stages [Figs. 1(b)–1(e)]. This indicates that the growth does not follow a three dimensional (3D) or Volmer–Weber mechanism, nor a layer-by-layer plus 3D islands, or Stranski–Krastanov mechanism. However, some variations of the surface topography are observed in the clusters or islands on local surface areas. These imply that the growth is more like a 2D mode, in agreement with a previous TEM study.[15] Figure 8 schematically shows cross sections of polyimide thin films at different Al deposition stages. In the schematics, the Al and polyimide interface is not scaled, nor are the Al islands.

The adsorbate–substrate interactions and adsorbate–adsorbate interactions play a key role in the Al growth. Sev-

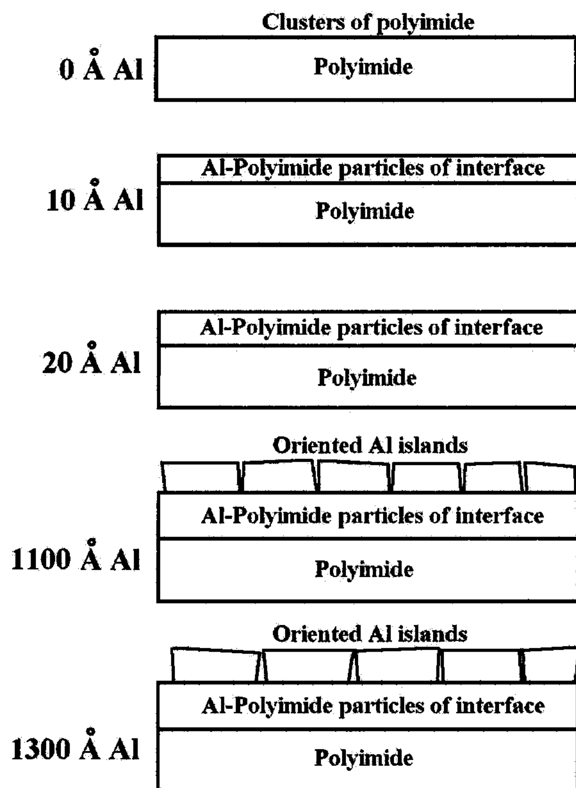

FIG. 8. Schematics of cross sections of polyimide thin films at different Al deposition stages.

eral other factors also influence the growth behavior, such as sample preparation, Al deposition rate, the specific chemistry of the polyimide substrate, and the polyimide substrate temperature during the Al growth. We note that a higher Al deposition flux (500 Å/s) would create 3D growth, as indicated in a previous TEM study.[15] We used a 10 Å/s deposition rate in this study, this was based on a consideration of obtaining a maximum film density on the Al thin films for a specific industrial application.

The primary purpose of the aluminum coatings under study is to provide visible light rejection while minimizing signal loss to a detector behind the film. To maximize light blocking efficiency, a number of depositions were performed at various deposition rates and their respective densities were determined. The resulting data show a very strong correlation between deposition rate and film density, with density leveling out around the bulk density of 2.7 g/cm^3 at a deposition rate of 8–10 Å/s. 10 Å/s provides good film density at a deposition rate well suited to the thickness under study, and was subsequently used for all Al films produced for this article. We have also conducted a study of Al growth on polyimide free standing films to examine variations of surface morphologies at different Al film thickness, as well as the resulted material properties. The results will be reported elsewhere.

Our XPS measurements are essentially consistent with previous XPS studies, and we would like to address two points combined with our AFM, FIB-SEM, and RBS results. First, we see that the initially deposited Al interacts with the carbonyl groups of polyimide and forms the interfaces of nanoparticles, as revealed in the AFM images [Figs. 1(b), 1(c), and Fig. 2]. At high film thickness, the deposited Al forms oriented crystalline islands, and the surfaces of the islands are covered by the oxidized layers of the small particles [Figs. 1(d)–1(f) and Fig. 3]. Small amounts of C and N are present on the surface, and we think that these are most likely hydrocarbon-related organic molecules created due to exposure to air. These two elements comprise about 15% and 1% of the surface concentration, respectively. There is no strong evidence to lead us to believe that these surface C and N arise from inside the polyimide. We note that this is different from a conclusion drawn from previous XPS and UPS studies[6] in which C and N from inside the polyimide diffused up through the grain boundaries of the crystalline Al thin films to form Al–C and Al–N complexes and covered the surface. The thickness of the crystalline Al layers was 170 monolayers in one study, which is much thinner than the Al layers we deposited in this study [Fig. 1(e)].

At the interface, the Al $2p$ line shows four features, where the dominant peak at 72.85 eV arises from the Al interacting with carbonyl groups of the polyimide. These features in the Al spectrum gradually smear out and disappear inside the polyimide, possibly indicating that the Al diffuses slightly into the polyimide. However, the metallic Al signal disappears prior to the oxidized Al forms, which indicates that if direct diffusion of unreacted Al metal has occurred, the Al has since chemically reacted with the polyimide. There is no Al clustering at this stage. The FIB-SEM image in Fig. 5 directly displays the interfacial formation of Al/polyimide when 1600 Å Al grows on 1100 Å polyimide. The thickness of the Al/polyimide interface will depend on several factors, such as the deposited Al thickness, deposition rate, sample preparation, etc. In this study, we have focused our attention on monitoring the morphology evolution at the early and later Al deposition stages, and we did not specifically investigate the effects of these different factors on the formation of the interface structures.

V. CONCLUSION

Atomic force microscopy, Rutherford backscattering spectroscopy, x-ray photoelectron spectroscopy, and focused ion beam scanning electron microscopy have been used to study Al growth, nucleation, and surface and interfacial structures on polyimide. At the initial growth, Al interacts with carbonyl groups of the polyimide to form interfacial structures of nanoparticles. The topography of the formed thin films at the initial stage is correlated to the surface morphology of polyimide. Subsequent Al growth creates crystalline islands with submicrometer size, exhibiting different orientations. Al growth on the polyimide follows a 2D-like fashion.

ACKNOWLEDGMENTS

Authors from Charles Evans & Associates would like to thank Dr. Thomas F. Fister, Dr. Kuo-Jen Chao, Dr. Robert W. Odom, and Dr. Patricia M. Lindley for their help in this study.

[1] *Polyimides: Fundamentals and Applications*, edited by M. K. Ghosh and K. L. Mittal (Marcel Dekker, New York, 1996).
[2] *Metallized Plastics: Fundamentals and Applications*, edited by K. L. Mittal (Marcel Dekker, New York, 1998).
[3] C. C. Parks, J. Vac. Sci. Technol. B **15**, 1328 (1997).
[4] T. P. Nguyen and J. L. Mansot, Thin Solid Films **283**, 135 (1996).
[5] W. Nabtikassega, P. Dannetun, O. Inganas, and W. R. Salaneck, Thin Solid Films **224**, 232 (1993).
[6] J. W. Bartha, P. O. Hahn, F. K LeGoues, and P. S. Ho, J. Vac. Sci. Technol. A **3**, 1390 (1985); P. S. Ho, P. O. Hahn, J. W. Bartha, G. W. Rubloff, and F. K. LeGoues, *ibid.* **3**, 739 (1985).
[7] H. Y. Tong, F. G. Shi, B. Zhao, S. O. Wang, M. Brongo, and P. K. Vasudev, Appl. Phys. A: Mater. Sci. Process. **65**, 287 (1997).
[8] E. Ettedgui, H. Razafitrimo, K. T. Park, and Y. Gao, J. Appl. Phys. **75**, 7526 (1994).
[9] E. Z. Kurmaev *et al.*, J. Vac. Sci. Technol. A **17**, 593 (1999).
[10] N. Miki, K. Tanaka, A. Takahara, and T. Kajiyama, J. Vac. Sci. Technol. B **18**, 313 (2000).
[11] H. Wickland, R. Talevi, Z. L. Bian, G. Nuesca, S. Sankaran, K. Kumar, R. E. Geer, and A. E. Kaloyeros, J. Vac. Sci. Technol. B **18**, 2463 (2000).
[12] S. R. Peddada, I. M. Robertson, and H. K. Birnbaum, J. Mater. Res. **9**, 504 (1994).
[13] A. N. Lachinov, T. G. Zangurenko, V. M. Kornilov, A. I. Fokin, I. V. Aleksandrov, and R. Z. Valiev, Phys. Solid State **42**, 1935 (2000).
[14] J. S. Cho, W. K. Chol, S. K. Koh, and K. H. Yoon, J. Vac. Sci. Technol. B **16**, 1110 (1998).
[15] J. F. Silvain, J. J. Ehrhardt, A. Picco, and P. Lutgen, in *Metallization in Polymers*, edited by E. Sacher, J. J. Pireaux, and S. P. Kowalczyk, ACS Symp. Ser. 440 (American Chemical Society, Washington, DC, 1990), p. 453.
[16] G. Danev, E. Spassova, and K. Popova, Thin Solid Films **278**, 301 (1993).
[17] H. M. Wu, Y. M. Zhu, Q. Luo, X. M. Yang, Z. H. Lu, and Y. Wei, J. Vac. Sci. Technol. B **14**, 1321 (1996).
[18] C. D. Dimitrakopoulos and S. P. Kowalczyk, Thin Solid Films **295**, 162 (1997).
[19] G. J. Szulczewski, T. D. Selby, K. Y. Kim, J. D. Hassenzahi, and S. C. Blackstock, J. Vac. Sci. Technol. A **18**, 1875 (2000).
[20] G. Padeletti, S. Pergolini, G. Montesperelli, A. D'Alessandro, F. Campoli, and P. Maltese, Appl. Phys. A: Mater. Sci. Process. **71**, 571 (2000).
[21] M. Nowicki, H. Kaczmarek, R. Czajka, and B. Susla, J. Vac. Sci. Technol. B **18**, 2477 (2000).